

Paper

Int'l J. of Aeronautical & Space Sci. 17(3), 296–314 (2016)

DOI: <http://dx.doi.org/10.5139/IJASS.2016.17.3.296>

Experimental and Computational Study on Separation Control Performance of Synthetic Jets with Circular Exit

Minhee Kim*

Central Research Institute, Korea Hydro & Nuclear Power Co. Ltd., Daejeon 34101, Republic of Korea

Byunghyun Lee**

Aero Technology Research Institute, Republic of Korea Air Force, Daegu 41169, Republic of Korea

Junhee Lee***

Department of Mechanical and Aerospace Eng., Seoul National University, Seoul 08826, Republic of Korea

Chongam Kim****

Department of Mechanical and Aerospace Eng., Seoul National University, Seoul 08826, Republic of Korea

Institute of Advanced Aerospace Technology, Seoul National University, Seoul 08826, Republic of Korea

Abstract

This paper presents experimental and computational investigations of synthetic jets with a circular exit for improving flow control performance. First, the flow feature and vortex structure of a multiple serial circular exit were numerically analyzed from the view point of flow control effect under a cross flow condition. In order to improve separation control performance, experimental and numerical studies were conducted according to several key parameters, such as hole diameter, hole gap, the number of hole, jet array, and phase difference. Experiments were carried out in a quiescent condition and a forced separated flow condition using piezoelectrically driven synthetic jets. Jet characteristics were compared by measuring velocity profiles and pressure distributions. The interaction of synthetic jets with a freestream was examined by analyzing vortical structure characteristics. For separation control performance, separated flow over an airfoil at high angles of attack was employed and the flow control performance of the proposed synthetic jet was verified by measuring aerodynamic coefficient. The circular exit with a suitable hole parameter provides stable and persistent jet vortices that do beneficially affect separation control. This demonstrates the flow control performance of circular exit array could be remarkably improved by applying a set of suitable hole parameters.

Key words: synthetic jet, flow control, vortex structure

Nomenclature

α = angle of attack
 C_d = sectional drag coefficient estimated from wake velocity deficit
 C_l = sectional lift coefficient estimated from airfoil

surface pressure distribution
 C_p = pressure coefficient ($\Delta P / (1/2 \rho_\infty U_\infty^2)$)
 C_μ = momentum coefficient according to flow velocity at synthetic jet exit ($\rho_\infty \overline{u_j^2} h / (1/2 \rho_\infty U_\infty^2 L)$)
 c = chord length
 D = diameter of circular exit

This is an Open Access article distributed under the terms of the Creative Commons Attribution Non-Commercial License (<http://creativecommons.org/licenses/by-nc/3.0/>) which permits unrestricted non-commercial use, distribution, and reproduction in any medium, provided the original work is properly cited.

© * Ph. D
** Ph. D
*** Ph. D Student
**** Professor, corresponding author: chongam@snu.ac.kr

f	= oscillation frequency of diaphragm
F^*	= reduced frequency according to synthetic jet oscillating frequency and characteristic length (fL / U_∞)
G	= gap of multiple serial circular exit
h	= depth of orifice
L	= characteristic length
m	= slope of pressure coefficient distribution ($(C_p - \text{constant}) / \ln(x / L)$)
ΔP	= difference between the measured pressure and the reference pressure
ΔC_l	= percentage of lift coefficient increase ($((C_{l_{jet\ off}} - C_{l_{jet\ on}}) / C_{l_{jet\ off}} \times 100)$)
$\Delta C_l / C_d$	= percentage of lift-to-drag ratio increase ($((C_l / C_{d_{jet\ off}} - C_l / C_{d_{jet\ on}}) / (C_l / C_{d_{jet\ off}} \times 100))$)
$Re\#$	= Reynolds number
U_∞	= freestream velocity
$\frac{u_j}{\bar{u}_j}$	= root mean square velocity of the issuing synthetic jet ($\sqrt{\bar{u}_j^2}$)
V_{pp}	= positive peak voltage and negative peak voltage
x	= chordwise distance from the leading edge
y	= spanwise distance from center line
z	= normal distance from wall
ρ_∞	= freestream density
A_{jet}	= suction or blowing amplitude, instantaneous peak velocity at orifice
δ	= boundary-layer thickness

1. Introduction

Synthetic jets have been widely used for a variety of purposes, such as flow control [1, 2], jet mixing enhancement [3], and heat transfer [4]. In particular, control of flow separation by means of synthetic jets is known to be quite effective under various flow conditions [5]. A synthetic jet periodically transports momentum from a jet cavity to an outside region, thus promoting the interaction with an external flow field by generating a series of jet vortices. The vortex formation process is quite important in a sense that it determines the level of overall flow control performance. Thus, studies on synthetic jets have focused on the vortex formation of a synthetic jet in a turbulent mixing layer and the assessment of its behavior under various conditions.

Many researchers and engineers produced experimental results in jet characteristics and jet vortex formation. Crook and Wood examined the behavior of synthetic jets under a quiescent condition, a cross-flow, and a boundary layer [6]. The quiescent condition means flow condition without freestream, and the cross-flow condition is flow under

freestream. They studied the delay of flow separation on a circular cylinder by using hotwire anemometry and flow visualization technique. Feng and Wang. investigated the flow separation control of a circular cylinder using a synthetic jet positioned at the front stagnation point by particle image velocimetry (PIV) technique [7]. They also controlled the wake behind a circular cylinder by a synthetic jet, and analyzed the vortex shedding modes and mechanism [8]. Amitay and Cannelle studied the evolution and transient behavior of finite span synthetic jets using hot wire anemometry and PIV technique. They also examined the effect of the slot aspect ratio on the development of a synthetic jet, and the spatial evolution of secondary three-dimensional vortical structures [9, 10].

At the same time, a number of numerical studies have also been carried out. Ravi et al. examined the formation and evolution of a synthetic jet, and compared the dynamical characteristics in quiescent and cross-flow conditions [11]. Rumsey et al. performed a study on synthetic jet flows entering into a turbulent boundary layer through a circular orifice [12]. W. Nitsche et al. studied flap separation control by introducing periodic excitation near a flap for high-lift configuration [13, 14]. Kim and Kim numerically investigated the frequency-dependent flow control mechanism of synthetic jets on an airfoil, and proposed multi-location synthetic jets to mitigate the unstable flow structure of a high-frequency jet [15]. Subsequently, Kim et al. applied synthetic jets to improve the aerodynamic performance of tilt-rotor UAV airfoils in hovering and transitional flight modes [16]. Zhong et al. examined the vortex structure produced by a synthetic jet in water, and presented the vortex roll-up criterion according to the Stokes length using experimental and numerical methods [17]. In addition, the flow physics associated with the interaction process between a circular synthetic jet and a laminar boundary layer was investigated by 3-D numerical simulations [18]. In the work by Kim et al., experimental and computational investigations on the characteristics of synthetic jets for different exit configurations under various flow conditions have been conducted [19]. Depending on vortex structure at jet exit, they considered two types of exit configurations: one is a conventional rectangular slot and the other is a series of circular holes. Comparative studies were then conducted for a quiescent condition, a cross flow field, and a forced separated flow. This study has revealed that overall jet characteristics and jet performance substantially depend on jet exit configuration. The circular exit array configuration and the three-dimensional oscillation of synthetic jets are promising for flow separation control. However, detailed flow characteristics for a flow separation control strategy have not

been fully investigated. At the same time, some issues, such as the vortex structure depending on jet exit configuration and a set of circular hole parameter producing an optimal jet performance, were also surfaced for the purpose of further investigation and practical implementation.

The present work is on the line of expanding the work by Kim et al. [19] and addresses the fore-mentioned issues with synthetic jets of circular exit under various flow conditions. Thus, the research objective is to investigate the local flow feature and vortex structure associated with circular synthetic jets, and determine an optimal range of the key design parameters of circular synthetic jets from the view point of flow control. In order to achieve such goal, the flow characteristics of a multiple serial circular exit are numerically investigated. Based on the observed flow features, detailed comparative studies are then conducted by changing the key design parameters, such as hole diameter, hole gap, the number of hole, jet array, and phase difference. In order to find an improved circular exit array, step-by-step experimental and numerical studies are conducted under various flow conditions. The characteristics of synthetic jet actuators are investigated by hot-wire measurement under a quiescent condition. The interaction of synthetic jets with a freestream is investigated by analyzing the vortical structure characteristics. Pressure distribution on an inclined flat plate is examined to assess the flow control characteristic under a forced separated flow condition. Finally, in order to verify the separation control capability, the improved design parameters of circular synthetic jets are applied to a NACA 64A210 airfoil, and the flow control performance is examined by measuring surface pressure coefficient, lift coefficient, and drag coefficient.

2. Numerical Methods

2.1 Governing equations

Accurate prediction of massively separated flow characteristics with or without turbulence models is still an extremely challenging task. By considering available computing power and required numerical accuracy, the present approach relies on solving Unsteady Reynolds-averaged Navier-Stokes (URANS) equations. It is known that URANS simulation combined with adequate turbulence models, such as the κ - ω SST turbulence model, can provide reasonably good solutions [20].

The incompressible governing equations are given by the continuity equation and the momentum equation for the conservation of mass and momentum, where the over-bar indicates a Reynolds-averaged quantity.

$$\nabla \cdot \bar{u} = 0 \quad (1)$$

$$\rho \frac{\partial \bar{u}}{\partial t} + \rho \bar{u} \cdot \nabla \bar{u} = -\nabla \bar{p} + (\mu + \mu_t) \nabla^2 \bar{u} \quad (2)$$

The governing equations were then solved in a time-accurate manner by employing the method of pseudo-compressibility, where τ is the pseudo-time and β is the pseudo compressibility parameter [21, 22].

$$\frac{\partial \bar{p}}{\partial \tau} = -\beta \nabla \cdot \bar{u} \quad (3)$$

The upwind differencing scheme based on flux-difference splitting, combined with the MUSCL approach, was used to calculate the convective term with a third-order spatial accuracy. The viscous fluxes were then centrally differenced by a second-order spatial accuracy, and the flow variables were updated by the LU-SGS time integration [23]. The turbulence model used in the present computations is the Menter's shear stress transport two-equation model, which has provided excellent predictions of flows involving separation [22, 24]. Also, Total Stress Limitation (TSL) method was employed to include the effect of flow transition [25]. All computations were performed with a finite volume-based in-house code that had been extensively validated [15, 16, 22].

2.2 Synthetic jet boundary conditions

A synthetic jet actuator is an oscillatory jet generator that requires zero-net mass input yet produces a non-zero momentum output. At CFDVAL2004, Rumsey et al. reported that, compared to experimental data, the velocity distributions near the orifice exit might exhibit some anomalies, but they also mentioned that global flow features could be captured with a reasonably good accuracy [20, 26]. In addition, Geissler studied the simplified boundary conditions for the simulation of flow control problems. They observed that the flow details between calculation and measurement do not fit completely, but the qualitative comparisons such as velocity profiles and lift polar are very similar [27]. Based on these reports, the suction/blowing-type boundary condition proposed by Kral et al., as in Eq. (4), was applied to the synthetic jet actuator [28]. The 'top hat' condition, wherein the spatial variation of the jet at the orifice was neglected, was employed to obtain computationally efficient results without compromising physical reality [15, 16, 29]. A perturbation to the flow-field was then introduced by the jet velocity where ξ denotes the streamwise direction, η denotes the spanwise direction, and ζ denotes the normal direction from the wall. \vec{u}_n is the velocity vector, and \vec{d}_{jet}

is a unit vector in the jet direction. The top hat boundary condition employed in this work can be expressed as follows.

$$\vec{u}_n(\xi = 0, \eta = 0, \zeta, t) = A_{jet} f(\zeta) \sin(\omega t) \vec{d}_{jet}, \quad f(\zeta) = 1 \quad (4)$$

3. Experimental Setup

3.1 Basic module design

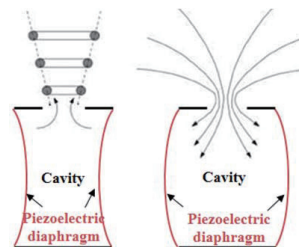
The piezoelectrically driven synthetic jets were used in experiments for light weight combinations of miniaturization. The piezoelectric diaphragm is made of a piezoceramic material (Piezo Systems PSI-5A4E). Its displacement is small and its operating condition is greatly influenced by the range of the oscillating frequency. To overcome this drawback and increase the volume change in the cavity, the dual diaphragm was adopted for higher jet velocity [30, 31]. A schematic of piezoelectrically driven actuators is shown in Fig. 1a. Jet momentum is produced by the volume change of the cavity by two piezoelectric diaphragms. Fig. 1b shows the manufactured synthetic jet module. Its weight and size is about 100g and 80 mm × 80 mm × 16mm, respectively. The basic outer components consist of acrylic parts, and the piezoelectric diaphragm is installed on both sides of the cavity. The outer acrylic components are fixed by screws and nuts to allow an easy replacement of the exit configuration. The bimorph-type piezoelectric disk manufactured by Piezo Systems was chosen based on the performance tests of several types of piezoelectric diaphragms. A piezoceramic material is coated onto the two layers of a circular metal plate with a diameter of 63.5 mm. The maximum free deflection of the disk is reported as ± 476 μm when the disk is vibrated at its resonance frequency. Performance tests by changing the input voltage were conducted to determine a suitable range of input voltage. Both single and dual diaphragms were activated, and laser displacement sensors (LB-70 series) were used to measure the deflection of each diaphragm. Experiments showed that the diaphragm displacement became larger as the input voltage increased. Considering

that voltage amplitude greater than $V_{pp} = \pm 200$ V caused cracks on the surface of the piezoceramic material, $V_{pp} = \pm 180$ V was chosen as the input voltage amplitude. In order to maintain the peak velocity, a sinusoidal waveform was used [31, 32]. The experimental frequency range of the synthetic jet was about $f = 50 - 200$ Hz considering the structural safety of the piezoelectric diaphragm.

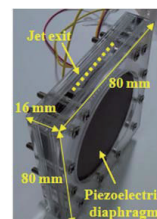
The jet velocity issuing from the exit was measured by an I-type single hot-wire. Single hot-wire anemometry with a 5 μm tungsten wire (Kanomax model 1011) was used in the constant temperature mode. A static calibration of the hot wire was carried out by placing a probe in the freestream of a subsonic wind tunnel (open jet type). The relationship between the voltage and the velocity was calculated based on King’s law. The instrumental uncertainty in the velocity measurement based on the accuracy of pressure transducer was found to be less than 0.134 Pa. The hot wire was installed on an auto-traverse system with an accuracy of 0.1 mm. The maximum relative uncertainty of the velocity ratio based on the turbulent intensity, U/U_∞ , is below 1 % within measurement range. Taking into account that the jet velocity oscillates, all velocity data were time-averaged with a period greater than 30s. A hot-wire probe of 3 mm off the central point of the exit hole was placed to prevent any suction effect near the exit. An I-type hot wire was then used for the measurements, only during the blowing phase, to prevent the directional ambiguity.

3.2 Inclined flat plate (configuration 1)

In order to study an improved exit configuration of synthetic jets, comparative experiments were conducted under a forced separated flow by changing hole gap and hole diameter. Fig. 2a shows the setup of the inclined flat plate for a wind tunnel test. A two-dimensional inclined flat plate was selected to simplify the separated flow condition. Owing to its geometric simplicity, other complex effects, such as curvature or uncertainty of upstream conditions, can be eliminated, and the location of forced separation is fixed. An inclined flat plate made of acrylic material was



(a) Dual-diaphragm actuator



(b) Manufactured synthetic jet module

Fig. 1. Schematics of piezoelectrically driven synthetic jet actuator

assembled to create a separated flow region on the rear plate. The incidence angle of the rear plate was 20° with respect to the front plate. The rear plate was 150 mm long and 200 mm wide. A single synthetic jet module was then installed near the starting point of flow separation. Due to the thickness of the synthetic jet module, the synthetic jet exit was located at about 8 mm downstream from the leading edge of the rear plate.

To examine the flow control phenomena, static pressure taps were installed along the center of the front and rear plate. Static pressure was then obtained using a net pressure scanner (Pressure Systems). The instrumental uncertainty in the pressure measurement with the pressure scanner was less than $\Delta C_p = 0.057$. All pressure data were time-averaged with a period greater than 30s, and the sampling frequency of pressure data was 10 Hz. Experiments were conducted using a subsonic wind tunnel (open jet type) with a test section of 200 mm \times 200 mm \times 1000 mm at the Wind Tunnel Laboratory of Seoul National University. The freestream velocity was measured by a pitot tube linked with a differential pressure transducer (MKS Instruments). The pitot tube was installed on the ceiling of the test section in front of the model. The freestream velocity was 10 m/s. Real-time pressure data were obtained by a 16-bit-A/D board and were processed by Labview 8.5 software (National Instruments Inc.). The instrumental uncertainty of the freestream velocity measurement with the pressure transducer was less than 0.134 Pa, and the turbulence intensity was less than 1%. Experimental range of frequency was $f = 50 - 150$ Hz. As a reasonable range of separation prevention [5], the following jet parameters were used: $0.75 \leq F+ \leq 2.25$ and $0.11 \% \leq C\mu \leq 0.543\%$.

3.3 Inclined flat plate (configuration 2)

Comparative experiments were conducted again under a forced separated flow to investigate an improved array of synthetic jets. Fig. 2b shows a typical wind tunnel test setup.

The test setup is similar to that of the previous experiment, except for the plate size and the wind tunnel type. An inclined flat plate made of acrylic material was installed to create a separated flow region on the rear plate. The rear plate was 400 mm long and 400 mm wide, and the incidence angle was 22° . The first array jet modules were located about 8 mm downstream from the leading edge of the rear plate, and the second array jet modules were installed 13mm and 42 mm behind the first array to examine the effect of multi-location synthetic jets. 32 static pressure taps were installed along the plate center as shown in Fig. 2b, and 16 spanwise pressure taps were located at 60 mm and 260 mm from the leading edge of the rear plate. The instrumental uncertainty in the pressure measurement with the pressure scanner was less than $\Delta C_p = 0.014$. All pressure data were time-averaged with a period greater than 30s. Experiments were then conducted using a subsonic wind tunnel(closed circuit type) with a test section of 1350 mm \times 950 mm \times 2440 mm at the Wind Tunnel Laboratory of Seoul National University. End plates were installed on both sides of the inclined flat plate to maintain a two-dimensional condition. A pitot tube was installed on the ceiling of the test section in front of the model. The freestream velocity was 20 m/s. The instrumental uncertainty in the freestream velocity measurement with pressure transducer was less than 0.134 Pa, and the turbulence intensity was less than 1%. The range of the oscillation frequency was $f = 50 - 200$ Hz, indicating a range of the jet parameters was $1.0. \leq F+ \leq 4.0$ and $0.010\% \leq C\mu \leq 0.063\%$. Other data acquisition instruments were identical to those of the previous experimental condition.

3.4 NACA64A210 airfoil model

Experiments were conducted on an airfoil at a high angle of attack to verify the flow control capability of the improved exit configuration and the synthetic jet array. Because NACA64A210 airfoil produced the leading edge stall, synthetic jet was located near the separation point to demonstrate the

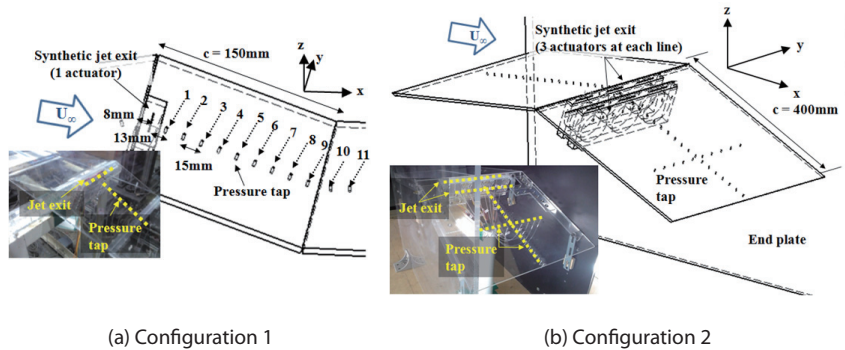
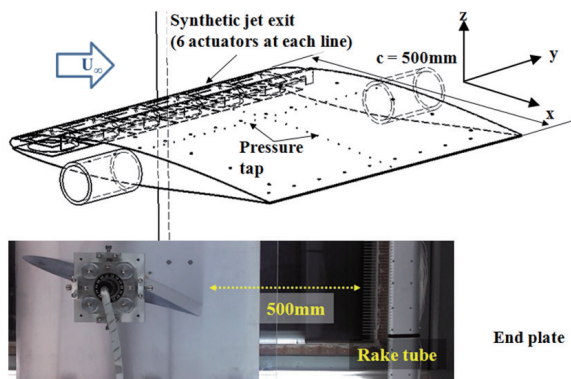


Fig. 2. Test setup of inclined flat plate

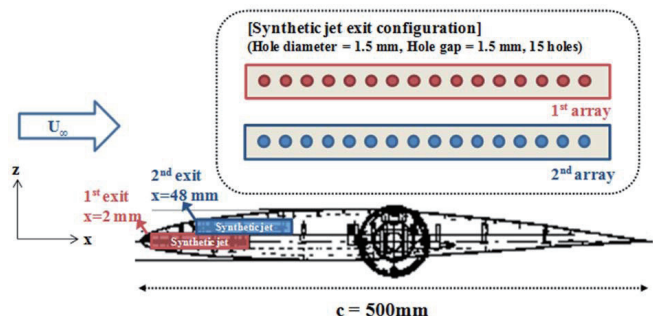
flow control capability [33-35]. Fig. 3 shows the wind tunnel setup(closed circuit type) using a NACA 64A210 airfoil with a 500 mm chord and 500 mm span. A detailed schematic of the experimental model is shown in Fig. 3a. Two arrays of synthetic jet modules were installed near the leading edge. The first array of synthetic jets was located very close to the leading edge ($x/c = 0.004$), and the second array was located 48 mm behind the leading edge ($x/c = 0.098$), reflecting the experimental result of the inclined flat plate. Each jet array was operated by six actuators. 32 Static pressure taps were located along the chord line of upper surface, and 16 spanwise pressure taps were located 149 mm ($x/c = 0.298$) and 325 mm($x/c = 0.65$) from the leading edge. Based on the measured surface pressure distribution, the sectional lift coefficient was calculated. A wake survey experiment was conducted to identify changes in drag according to the flow control. Fig. 3a shows a wake survey system to measure the velocity deficit from the total pressure difference. Each probe was connected to a net pressure scanner (Pressure Systems). The wake survey was done along the mid-span location at $x/c = 1$ from the trailing edge, and the sectional drag coefficient was calculated from the velocity deficit. End plates were installed on both sides of the airfoil to maintain a two-dimensional flow condition, and a stepper motor system was installed to change the angle of attack. The freestream velocities were 20 m/s and 30 m/s. The range of the operating frequency was $f = 50 - 200$ Hz, indicating a range of the jet parameters was $1.25 \leq F+ \leq 5.0$ and $0.008\% \leq C\mu \leq 0.050\%$. Other data acquisition instruments were identical to those used in the previous experiments.

4. Results and Discussions

4.1 Flow characteristics of synthetic jet with circular exit



(a) Schematics of NACA64A210 airfoil model



(b) NACA 64A210 airfoil test setup

Fig. 3. Test set up of NACA 64A210 airfoil model

The flow control effect of a multiple serial circular exit was investigated by examining the local flow feature, vortex structure, and wall shear stress distributions.

4.1.1 Code validation

Cross flow experiments with circular exit configuration were used for code validation [19]. In experiments, the synthetic jet was installed at the bottom of wind tunnel, located at 60 cm from the wind tunnel nozzle. The mean velocity profile was measured along the streamwise and spanwise directions by using the hot wire anemometry and auto traverse system. The geometric details and experimental data for test configuration can be found in Ref. 19. As depicted in Table 1, the circular exit has 7 circular holes, which is composed of 1.5 mm hole diameter and 1.5 mm hole gap. The Reynolds number based on the circular hole diameter is 1,000, the freestream velocity is 10 m/s, the jet frequency is fixed at 50 Hz, and the maximum velocity of the synthetic jet is 40 m/s. The boundary conditions of Eq. (4) can be then determined from the flow condition.

The computational coordinate system is shown in Fig. 4. The X-direction is the streamwise direction, the Y-direction is the spanwise direction of the exit, and the Z-direction is the normal direction from the wall. The origin of the coordinate is the center of the span. Fig. 5 shows the computational domain and boundary conditions used in the simulation. The inlet of the flow domain was located at the 150 mm upstream of the jet exit, and the outlet was set at the 450 mm downstream of the jet exit. The height and width of the computation domain were 300 mm and 250 mm, respectively.

Since the flow field was symmetric with respect to the XZ plane, only a half of the flow field was modeled to save the computational time. The inlet condition was specified using the steady mean velocity profiles of a fully turbulent incompressible flow. A symmetric boundary condition was

used on the both side of the XZ plane. The outlet pressure condition was employed at both the flow outlet domain and the surface opposite to the wall. The mesh type around the jet exit is a structured mesh, and the numbers of grid points

are 49 points (7 X 7) in the inner circle. The number of grid points between two adjacent holes are 15 points along the Y-axis.

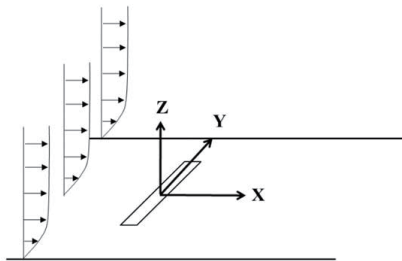


Fig. 4. Computational coordinate system

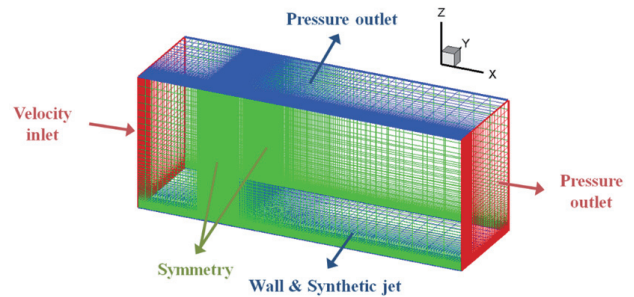


Fig. 5. Mesh and boundary conditions

Table 1. Circular hole configurations for experimental study

Exit type	Total exit area (mm ²)	Total exit perimeter (mm)	Total number of circular hole	Exit configuration
1-1	12.57	50.27	16	
1-2	12.57	32.99	7	
1-3	12.57	25.13	4	
2-1	12.57	32.99	7	
2-2	12.57	32.99	7	
2-3	12.57	32.99	7	
3	25.14	65.98	14	
4	26.94	70.69	15	

Verification study has been performed in term of grid refinement and time step sensitivity. Fig. 6 shows comparison of centerline velocity profiles. The X-axis is the ratio of freestream, and the Y-axis is the ratio of displacement thickness. The δ_0 means displacement thickness of flat plate without synthetic jet. From the comparison of the computed results depicted in Fig. 6a, the differences between fine mesh and medium mesh are found to be less than 2%, which is thought to be adequate for reliable computations. Thus, the mesh systems of 13 million grid points were considered for the circular exit calculation. With the chosen grid system, time-step sensitivity test was also conducted. In order to maintain sufficient temporal accuracy, sub-iterations were carried out with respect to pseudo-time until the maximum flow divergence of the converged solution at the fixed physical time became less than 1.0×10^{-5} . Three levels of different time steps were tested: 60, 90, and 120 steps per synthetic jet period. Fig. 6b shows the velocity profiles according to the number of time steps. The computational differences between 90 and 120 time steps were less than 2 percent, indicating that 90 time steps could adequately resolve the time-dependent nature of the flow fields within the URANS formulation. Computed results were then obtained after reaching a sufficient level of time-periodic behavior. With the chosen grid system and time step, the time-averaged velocity profiles of the boundary layer are compared with experimental data along the downstream direction, as shown in Fig. 6c. The computed results show a reasonable agreement with experimental data when synthetic jet is actuated. Thus, the numerical simulation is believed to be

capable of simulating the behavior of synthetic jets for the cross flow condition.

4.1.2 Numerical results and analyses

In order to investigate the interactions between the synthetic jet and the freestream, time sequences of iso-surface vorticity and velocity magnitude contours are examined, as shown in Fig. 7. Since flow structures at suction phase are not significantly different from those at blowing phase, blowing phase (phase $0^\circ - 180^\circ$) results are examined. From the flow characteristics in the quiescent condition, it is observed that a vortex ring is generated at each hole and moves along the normal direction from the wall [19]. The interactions between serial vortex rings of the spanwise direction and freestream are as follows. First, the serial vortex rings along the spanwise direction uniformly grow during phase $60^\circ - 90^\circ$. At phase 120° , as a result of the interactions between the serial vortex rings with an external flow field, jet vortices produce along the spanwise direction and develop to the streamwise direction. At phase 150° , the size of the resulting jet vortices along the spanwise direction becomes smaller, and a clockwise rotating flow is locally observed at the exit end. As shown in the velocity magnitude contours of iso-surface vorticity, the velocity of the clockwise rotating flow is larger than that of the jet vortices along the spanwise direction. Two flow characteristics are thus observed from the interactions: one is the jet vortices along the spanwise direction, and the other is the clockwise rotating flow at the exit end. By the jet vortices along the spanwise direction, the flow uniformly develops to the streamwise direction, and

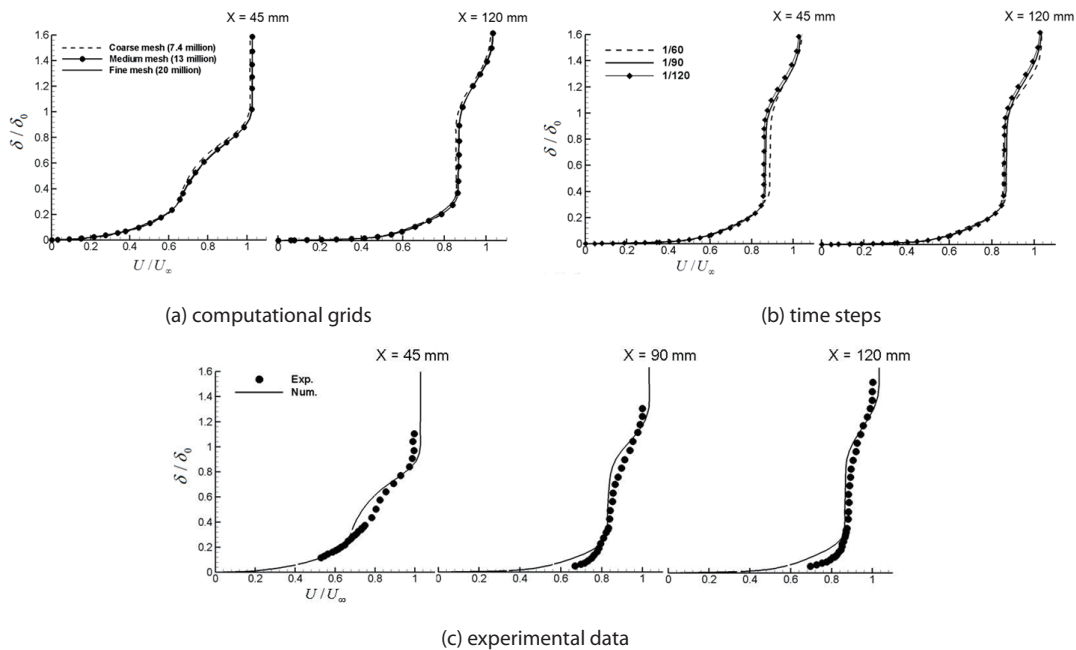


Fig. 6. Comparison of centerline velocity profiles at $y = 0$

affects to the downstream. On the other hand, the clockwise rotating flow produces a larger local velocity at the exit end at phase 150°.

The variation in wall shear stress can be a useful indicator to examine the effect on flow separation delay [18]. The smaller the decrease of the wall shear stress ratio, the more the flow field can preserve the jet vortical structure. From this perspective, the flow control effect of the circular exit configuration was evaluated by comparing the time-averaged wall shear stress distributions. Fig. 8 shows the ratio of the jet-on wall shear stress (τ_{wall}) to the jet-off wall shear stress (τ_{w_ref}) along the spanwise direction at several downstream locations. The streamwise locations are 5, 20, 50, 80, 120, and 200 mm from the origin, respectively. The spanwise locations are from $Y = 0$ mm to $Y = 40$ mm to cover from the exit center ($Y = 0$ mm) to the exit end ($Y = 25$ mm). At $X = 5$ mm, the wall shear stress ratio is highly oscillatory due to the hole gap effect. The maximum peak values appear at the center of each circular hole, while the minimum peak values are located between two adjacent holes. The value at the exit end is higher than that of exit center but it is quickly decreased along the downstream. This means that the flow structure at the exit end affects the initial jet strength. From $X = 20$ mm to the downstream direction, the drop of the wall shear stress ratio along the spanwise direction is smaller than that at the exit end. As a result, the overall flow structures along the spanwise direction become sustainable to the downstream.

In conclusion, the circular exit produces the jet vortices along the spanwise direction and the local clockwise rotating flow at the exit end as a result of the interactions with an external flow field. The jet vortices of the spanwise direction have the effect of maintaining the initial vortex produced by synthetic jet, and the clockwise rotating flow at the exit end yield a positive effect in strengthening the initial jet vortex.

4.2 Characteristics of circular synthetic jet according to design parameter

4.2.1 Effect of hole diameter

Table 1 shows a set of circular hole configurations for

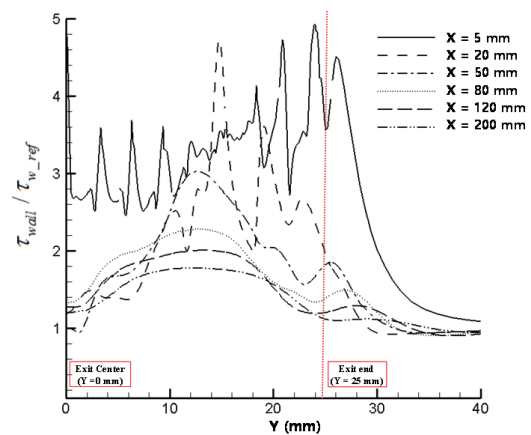


Fig. 8. Time-averaged distributions of wall shear stress ratio

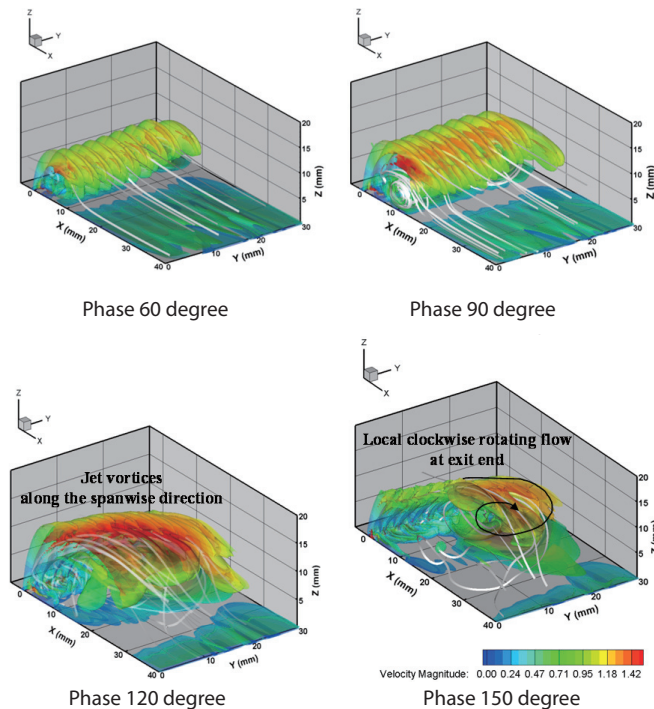


Fig. 7. Time sequences of iso-surface vorticity and velocity magnitude contours at blowing phase

experimental study. Exit types 1-1, 1-2, and 1-3 were used to investigate the effect of the hole diameter under the same total cross-sectional area condition (see Table 1). All of the exit configurations have the same orifice depth and total cross-sectional area. Fig. 9 shows the RMS jet velocities of exit types 1-1 ($D = 1$ mm), 1-2 ($D = 1.5$ mm), and 1-3 ($D = 2$ mm), measured at a height of $z = 3$ mm in a quiescent condition. The RMS jet velocity of exit type 1-3 is higher than that of the others over the entire frequency range.

The jet momentum (or the RMS jet velocity) according to the hole diameter is related to the hole perimeter and

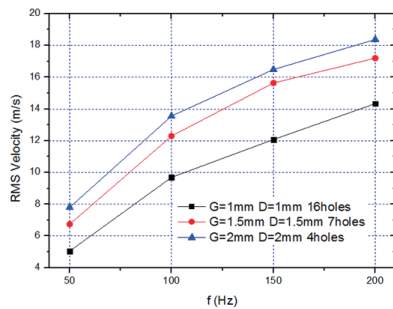


Fig. 9. RMS jet velocity (exit type 1-1, 1-2, and 1-3)

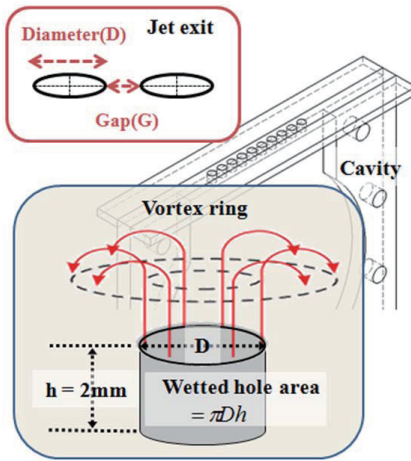
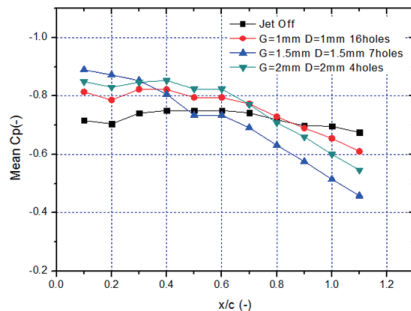
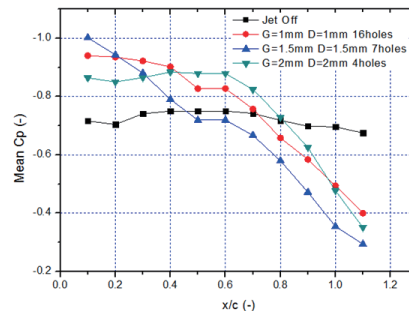


Fig. 10. Wetted hole area and vortex ring



(a) $C_{\mu} = 0.109, F^+ = 0.75$ ($f = 50$ Hz)



(b) $C_{\mu} = 0.331, F^+ = 1.5$ ($f = 100$ Hz)

Fig.11. Cp distribution on the rear plate (exit type 1-1, 1-2, and 1-3)

the wetted hole area. Fig. 10 defines the schematics of the wetted hole area in circular exit surface. Because of viscous loss in the wetted hole area, the jet momentum of exit type 1-1 is lowest. At the same time, the wetted hole area is proportional to the hole perimeter, and the effective area covered by the vortex ring produced from each hole is also proportional to the hole perimeter. Because the vortex ring plays an important role in enhancing the degree of mixing [26-29], both the jet momentum (or the RMS jet velocity) and the effective area of the vortex ring (or the hole perimeter) should be taken into account. Exit type 1-3 ($D = 2$ mm) has the smallest hole perimeter but produces the highest RMS velocity, indicating that it provides the smallest effective area covered by the vortex ring and the largest jet momentum. On the other hand, exit type 1-1 ($D = 1$ mm) has the largest hole perimeter and produces the lowest RMS velocity, thus it provides the largest effective area covered by the vortex ring and the smallest jet momentum.

Based on the above experimental observation in the quiescent condition, experiments over an inclined flat-plate (configuration 1 in Fig.2a) were conducted to find an adequate hole diameter that yields better flow control performance under a freestream velocity of $U_{\infty} = 10$ m/s. In order to evaluate the level of the pressure recovery of the rear plate, C_p slopes of exit types 1-1, 1-2, and 1-3 are compared along the centerline of the rear plate when $f = 50$ Hz and 100 Hz, as shown in Fig. 11. The higher the slope of the pressure coefficient curve is, the more the rear plate can recover the pressure. Exit type 1-1 ($D = 1$ mm), which has the smallest jet momentum and the largest wetted hole area, doesn't provide high pressure recovery along the downstream. On the other hand, Exit type 1-3 ($D = 2$ mm) which has the largest jet momentum and the smallest wetted hole area, doesn't show better flow control performance than that of Exit type 1-2 ($D = 1.5$ mm). Exit type 1-2 with $G, D = 1.5$ mm provides the highest pressure slope, suggesting that the performance of the circular jet with $D = 1.5$ mm is better than the others for separation control. For the purpose of effective flow control,

the jet momentum should be higher and the effective area of the vortex ring needs to be larger. From this perspective, exit type 1-2 ($D = 1.5$ mm) is chosen as a reasonable trade-off for this experimental configuration.

4.2.2 Effect of hole gap

In order to analyze the vortex structure, numerical simulations were performed by changing the hole gap (G) of the circular exit in a cross flow condition. The flow conditions are the same as the code validation case in Section 4.1.1. In order to maintain the same geometrical condition for each jet configuration, jet velocity and the number of hole were changed for the same total jet momentum and span length. The flow characteristics were then examined for the

hole gaps of 0.75, 1.5, and 3 mm (exit type 2-1, 2-2, and 2-3) with the same hole diameter of 1.5 mm. Fig. 12 shows the comparison of flow structures according to the hole gap at phase 120° . The left side is the iso-surface vorticity and velocity magnitude contours, and the right side is vorticity magnitude contours at the planes of $X = 5$ mm and $Z = 1$ mm, respectively. In the case of $G = 0.75$ mm, the velocity magnitude is larger than other cases and the vorticity magnitude increases toward the exit end. For $G = 3$ mm case, on the other hand, the velocity magnitude is smaller but the vorticity magnitude distribution is relatively uniform along the spanwise direction. This indicates, combined with the result in Section 4.1.2, the local clockwise rotating flow with a larger jet velocity at the exit end becomes significant

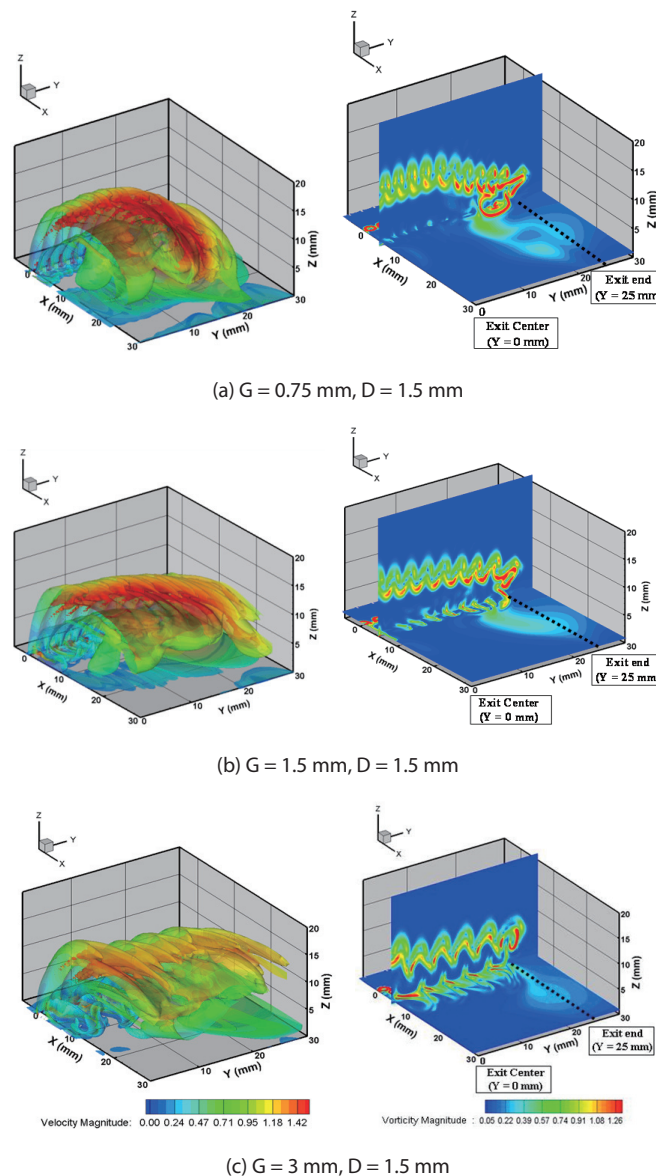


Fig. 12. Comparison of flow structure according to hole gap at phase 120°

as the hole gap decreases, while the uniform jet vortices with a smaller jet velocity along the spanwise direction are major characteristics as the hole gap increases. Fig. 13 is the streamwise distribution of the time-averaged wall shear stress ratio to compare the flow control effectiveness on the downstream flow field [19]. The horizontal axis indicates the streamwise locations of $X = 20, 50, 80, 120,$ and 200 mm from the origin, respectively. The vertical axis is the averaged values from $Y = 0$ to 40 mm at each streamwise location. In the case of $G = 0.75$ mm, the high peak of the wall shear stress ratio is quickly decaying along the streamwise direction. For $G = 3$ mm case, the wall shear stress ratio is relatively small but more persistent. Combined with the result of Section A-2, this suggests that the circular exit with small gap favorably affects strengthening the initial vortex produced by synthetic jet but is not effective in maintaining the initial strength to the downstream. On the other hand, the circular exit with large gap is not so effective in strengthening the initial vortex but favorably interacts with the freestream to maintain the initial vortex to the downstream. Therefore, the case of G1D1 is an appropriate trade-off to produce a strong and more sustainable initial vortex.

In order to compare the flow control capability depending on the hole gap, the time-averaged pressure coefficients

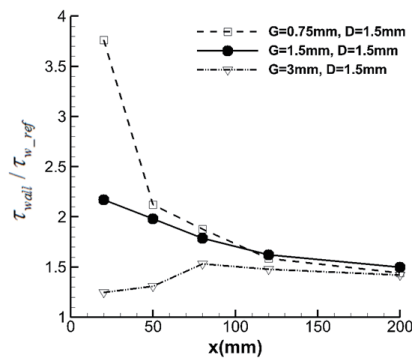
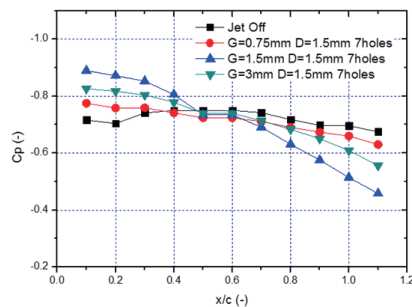
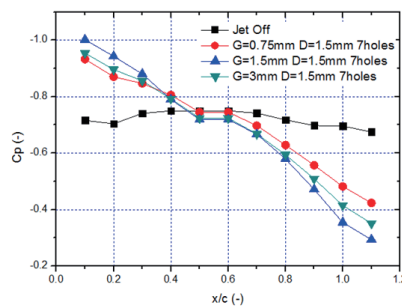


Fig. 13. Time-averaged streamwise distributions of wall shear stress ratio depending on the hole gap



(a) $C_{\mu} = 0.109, F^+ = 0.75$ ($f = 50$ Hz)



(b) $C_{\mu} = 0.331, F^+ = 1.5$ ($f = 100$ Hz)

Fig. 14. Cp distribution on the rear plate (exit type 2-1, 2-2, and 2-3)

were examined at inclined flat-plate experiments (configuration 1 in Fig. 2). Exit types 2-1, 2-2, and 2-3 (see Table 1) were used to investigate the effect of the hole gap under the same exit area and hole diameter condition. Fig. 14 represents the pressure coefficient distribution of exit type 2-1, 2-2, and 2-3 along the rear plate. Exit 2-2 with $G, D = 1.5$ mm provides the highest pressure coefficient slope, indicating that the performance of the circular jet G1D1 is better than the others for separation control. In case of $f = 100$ Hz (Fig 14b), exit type 2-2 clearly provides better performance for flow control. Based on the numerical and experimental results, it is observed that a suitable hole gap ($G = 1.5$ mm) for this experimental configuration can beneficially change the local flow feature and vortex structure for effective flow control.

4.2.3 Effect of number of holes

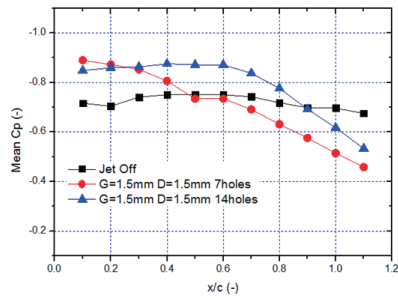
Exit type 3 of Table 1 was used to verify sufficient flow control area along the spanwise direction with $G = 1.5$ mm, $D = 1.5$ mm. Fig.15 compares exit type 2-2 and exit type 3 to examine the maximum allowable number of exit holes for each synthetic jet module (configuration 1 in Fig. 2). Exit type 3 has the maximum number of exit holes (14 holes), while the hole gap and hole diameter are identical to that shown in exit type 2-2. Because more circular holes make more mixing vortices along spanwise direction, the net flow control capability of exit type 3 is better than that of exit type 2-2.

4.2.4 Effect of jet array and phase difference

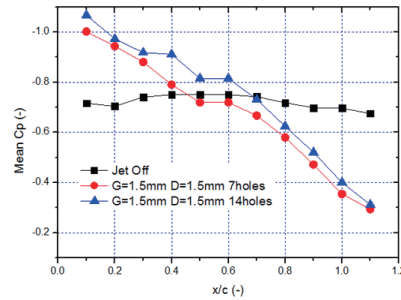
The inclined flat-plate experiments (configuration 2 in Fig. 2) were performed to examine the effects of the jet array type and oscillation phase on the flow control capability. Table 2 shows two types of synthetic jet arrays (single- and dual-array type) with different locations and array gaps. Flow control experiments with dual arrays were performed to examine the effect of multiple locations along the streamwise direction. One is the minimum gap (the second single array is 21 mm behind the separation point) due to the

thickness of the synthetic jet module, and the other is 50 mm

behind the separation point. In addition, jet oscillation types



(a) $C_\mu = 0.109$, $F^+ = 0.75$ ($f = 50$ Hz)



(b) $C_\mu = 0.331$, $F^+ = 1.5$ ($f = 100$ Hz)

Fig. 15. Cp distribution on the rear plate (exit type 2-2 and 3)

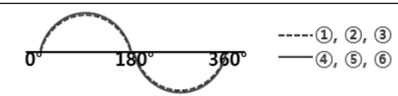
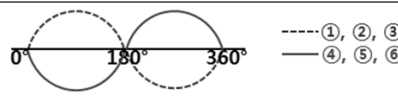
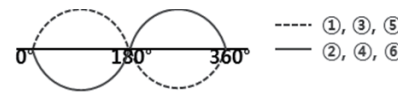
Table 2. Types of synthetic jet array

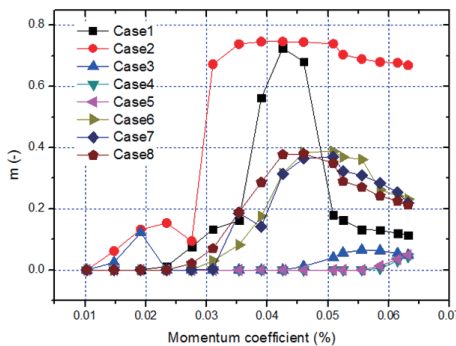
Type	Synthetic jet array (top view on the rear plate)	Array type
1		Single array
2		Dual array (13 mm gap)
3		Dual array (42 mm gap)
4		Single array
5		Single array
6		Dual array (46 mm gap)

are shown in Table 3. Exit type 3 in Table 1 was adopted for this experiment.

In an effort to understand the flow control capability quantitatively, the slope of the C_p curve (m) on the rear plate is compared according to the oscillation frequency and phase difference, as shown in Fig. 16. Regressions of all C_p curves were performed using an equation. The x-axis is the momentum coefficient (C_{μ}) and the y-axis is the C_p slope (m) distribution. Table on the right side explains the oscillation phase, and high-performance cases are highlighted. The pressure recovery slope is adopted as an index of flow control. A higher C_p slope means a higher pressure recovery. The single-array actuator with a 180° phase difference exhibits the best performance throughout the range of actuating frequency ($100 \text{ Hz} \leq f \leq 200 \text{ Hz}$). In addition, the dual-array actuators with a proper choice of array distance (Type 3 in Table 2) demonstrate stable performance regardless of the phase difference. In both single- and dual-array jets, 180° phase difference yields enhanced results because the phase shift of two-segmented slots facilitates flow mixing. As reported in earlier work [36], three-dimensional oscillation yielded beneficial interaction between adjacent actuators.

Table 3. Types of synthetic jet oscillation

Type	Oscillation phase	Comments
1		Identical phase of all actuators
2		180° phase difference along the streamwise direction
3		180° phase difference along the streamwise and spanwise direction



4.3 Verification of separation control capability

4.3.1 Synthetic jet-off

Before verifying the flow control performance of the synthetic jets on the NACA 64A210 airfoil, basic flow characteristics were undertaken by changing the angle of attack. Fig. 17 presents the mean and standard deviation of CP distributions on the airfoil upper surface according to the angle of attack at $Re\# = 6.67 \times 10^5$ and 1.0×10^6 . Though C_p was measured by the interval of $\alpha = 1^\circ$, a couple of meaningful flow characteristics are displayed. A constant pressure region starts to appear near the leading edge at $\alpha = 12^\circ$, implying that a separation bubble begins to grow over the stall angle [37, 38]. A higher angle of attack makes the separation bubble larger, leading to a flat C_p distribution along the airfoil upper surface. At the same time, the standard deviation of C_p becomes suddenly larger when the stall angle is imminent, indicating that the flow becomes unstable before the separation bubble starts to grow near the leading edge.

Figure 18 shows aerodynamic coefficients (C_l and C_d) by integrating the C_p distribution over the airfoil surface and the wake velocity deficit. This confirms again that the stall of the NACA 64A210 airfoil starts near $\alpha = 12^\circ$, and as

Case	Array type	Phase type
1	Single array	Identical phase of all actuators
2	Single array	180° phase difference along the spanwise direction
3	Dual array (gap 13 mm)	Identical phase of all actuators
4	Dual array (gap 13 mm)	180° phase difference along the chordwise direction
5	Dual array (gap 13 mm)	180° phase difference along the chordwise and spanwise direction
6	Dual array (gap 42 mm)	Identical phase of all actuators
7	Dual array (gap 42 mm)	180° phase difference along the chordwise direction
8	Dual array (gap 42 mm)	180° phase difference along the chordwise and spanwise direction

Fig. 16. Slopes of C_p curves (m) according to jet array and phase difference

a result, lift force decreases and drag force increases after the stall angle. Combined with the previous experimental results, the objective of the present flow control is to improve aerodynamic performance and to reduce pressure fluctuation at the leading edge by controlling the leading edge stall.

4.3.2 Synthetic jet-on

In order to control the leading edge stall on the NACA 64A210 airfoil, experiments were conducted by applying the design parameters obtained from the previous experiments. The basic outer components of synthetic jet module were manufactured by using aluminum alloy instead of acrylic parts, and exit type 4 in Table 1 was adopted for exit

configuration. Oscillation type 3 in Table 3 was adopted for phase difference, and array type 4, 5 and 6 in Table 2 were used for synthetic jet array.

Unlike the case of the inclined plate, separation control over the NACA64A210 airfoil present additional challenges since curvature effect can be significant and the upstream condition (laminar, transitional or turbulent) is also important. Thus, the design parameters obtained from the previous experiments as a means of maximizing flow control performance, were checked again. Flow control characteristics according to the design parameters of synthetic jets were compared with the baseline case ($\alpha = 12^\circ - 20^\circ$ in Sec. 4.3.1).

Figure 19 shows the effect of the synthetic jet array along

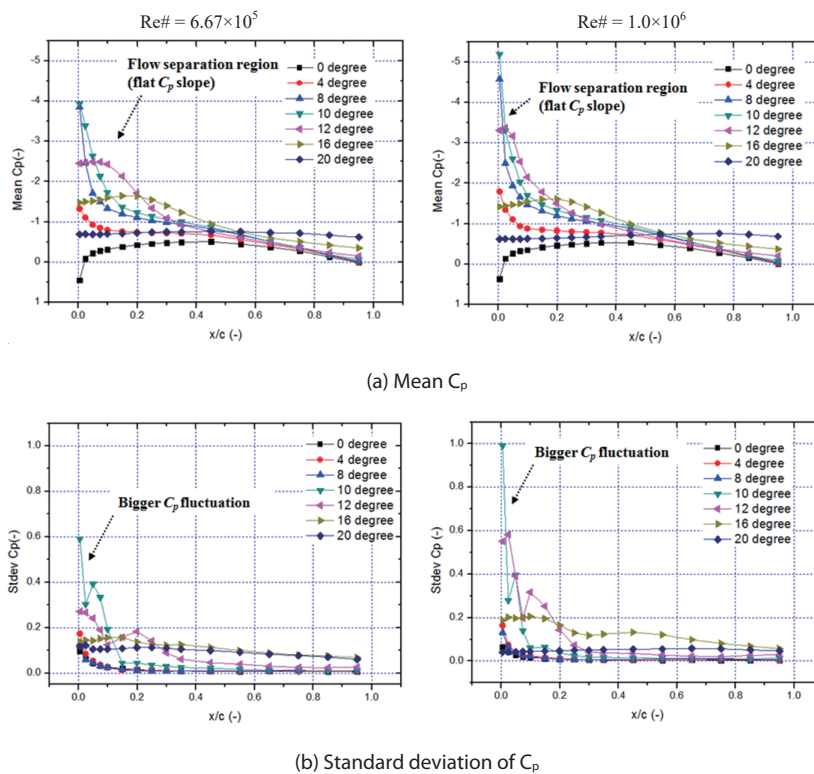


Fig. 17. Pressure distributions on the upper surface of NACA 64A210 (synthetic jet-off)

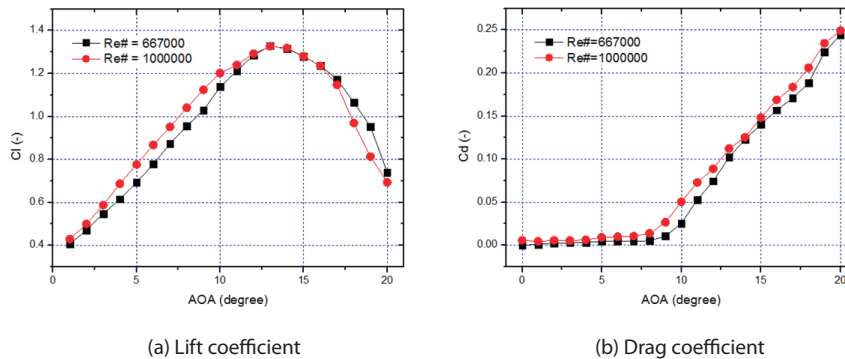


Fig. 18. Aerodynamic force of NACA 64A210 (synthetic jet-off)

the chordwise direction for $\alpha = 12^\circ$ and 20° . Figs. 19a and 19c represent the results when the airfoil stall begins ($\alpha = 12^\circ$), and Figs. 19b and 19d are the results for a fully separated condition ($\alpha = 20^\circ$). The mean C_p indicates the overall performance of flow control and the standard deviation of C_p represents the level of flow fluctuation (or flow stability). In the case of single-array synthetic jets, array type 4 yields the desired pressure recovery at the leading edge but array type 5 is not effective because the jet location is away from the separation point. This result confirms again that the proper location for separation control should be at or close to the separation point. For the dual-array actuation of type 6, overall aerodynamic performance is similar to that of

the single-array actuation of type 4. The benefits of dual-array actuation can be found in terms of the flow stability. In the mean C_p distribution, both the single array (array type 4) and dual array (array type 6) yield quite a similar flow control performance, as shown in Figs. 19a and 19b. However, the dual array is more favorable for suppressing flow fluctuation near the leading edge at high angles of attack, as shown in Figs. 19c and 19d. This result verifies again that multi-location synthetic jets have a beneficial effect of mitigating the unstable flow structure of a high-frequency jet [15]. From the results, it is demonstrated that the dual-array actuator (array type 6) with a 180° phase difference (oscillation type 3) is suitable in terms of flow

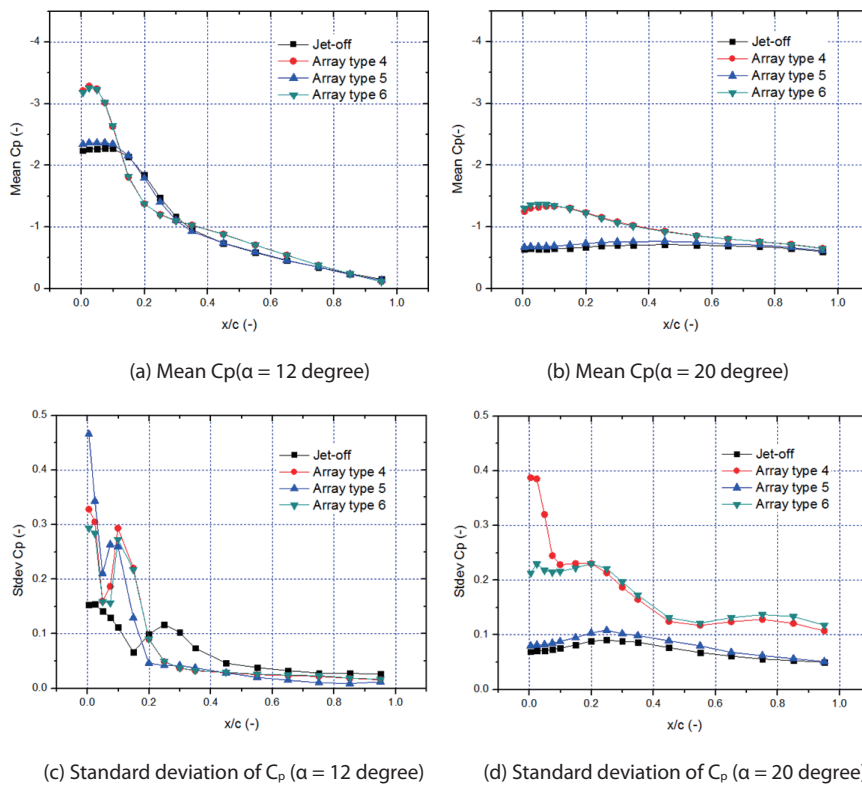


Fig. 19. C_p distribution depending on array type ($Re\# = 6.67 \times 10^5$, $C_\mu = 0.031$, $F+ = 3$)

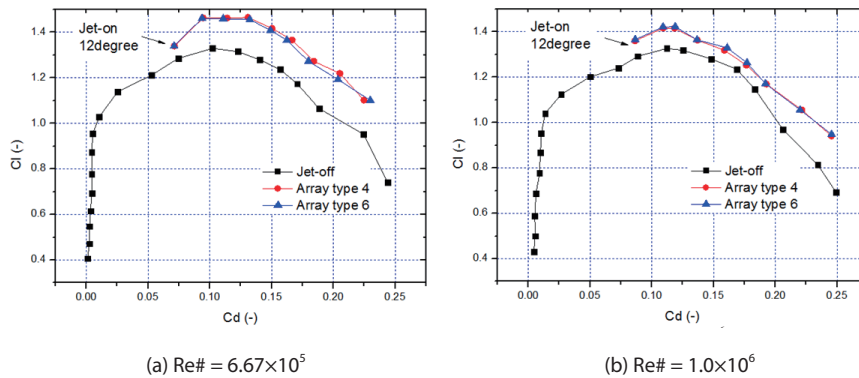


Fig. 20. Drag polar curve of NACA 64A210 ($C_\mu = 0.031$, $F+ = 3$)

control and flow stability.

Figure 20 shows the drag polar of the NACA 64A210 airfoil when $f = 120$ Hz. Based on the previous results, exit type 3 of Table 1, array type 6 of Table 2, and oscillation type 3 of Table 3 were adopted. Though not presented here, similar behavior can be obtained in terms of aerodynamic performance throughout the oscillation frequency range of $f = 100 - 200$ Hz. By operating the synthetic jets above the stall angle ($\alpha = 12^\circ$), the drag polar curve is significantly shifted toward the better position. These results confirm, together with all of the previous comparisons, that the synthetic jet system with well-selected design parameters is an effective tool for controlling separated flows.

5. Conclusion

The flow characteristics of synthetic jets with a circular exit were investigated using both experimental and numerical methods under various flow conditions to investigate the local flow feature and vortex structure, and identify the key design parameters from the view point of separation control. In order to achieve the goal, the flow characteristics of a multiple serial circular exit in the cross flow condition were numerically investigated. As a result of the interactions with an external flow field, the serial vortex rings produced the jet vortices along the spanwise direction and the local rotating flow at exit end, which played the role of making the initial vortex produced by synthetic jets more strong and sustainable. In order to determine the design parameters of circular exit array, step-by-step comparative studies were then conducted according to the hole diameter, the hole gap, the number of holes, the synthetic jet arrays, and the phase difference. First, experiments were carried out to examine the effect of the hole diameter under the quiescent condition and the forced-separated flow condition. Because both the jet momentum and the effective area of the vortex ring should be taken into account for flow control, the hole diameter of $D = 1.5$ mm was selected as a reasonable trade-off. Second, numerical and experimental studies were investigated by changing the hole gap. In order to maintain strong and more sustainable vortical structure, the hole gap of $G = 1.5$ mm was chosen, which can beneficially change the local flow feature and maintain the vortex structure for effective flow control. The flow control capability depending on the hole gap also verified in inclined flat-plate experiments. Then, the maximum allowable number of exit holes for each jet module was examined under the fully separated flow condition. More circular holes produced more

mixing vortices along the spanwise direction, which can enhance the net flow control capability with the same hole diameter and hole gap. Finally, the inclined flat-plate experiments were performed to examine the effects of the synthetic jet array type and oscillation phase on the flow control capability. By comparing the pressure distribution and pressure recovery, the single-array actuator with a 180° phase difference provided the best performance throughout the range of actuating frequencies. In addition, stable flow structure could be achieved by using the dual-array actuators. The flow control performance was verified for the separated flow condition on the NACA 64A210 airfoil by applying the design parameters obtained from the experiments and computations. The aerodynamic performance was significantly improved and pressure fluctuation near the leading edge was substantially reduced by controlling the leading edge stall.

Based on the experimental and numerical comparisons, it is observed that the exit configuration should be regarded as an important design factor, and the flow control performance of the circular exit can be significantly improved by applying the proposed hole parameters of synthetic jets.

Acknowledgement

We acknowledge the financial support from the Defense Acquisition Program Administration and the Agency for Defense Development (UC100031JD), and Ministry of Science, ICT & Future Planning through the project EDISON (NRF-2011-0020559). We also appreciate the financial supports provided by the program of Development of Space Core Technology (NRF-2015M1A3A3A05027630) through the National Research Foundation of Korea funded by the Ministry of Science, ICT and Future Planning.

References

- [1] Amitay, M., Smith, D. R., Kibens, V., Parekh, D. E. and Glezer, A., "Aerodynamic Flow Control over an Unconventional Airfoil Using Synthetic Jet Actuators", *AIAA Journal*, Vol. 39, No. 3, 2001, pp. 361-370.
- [2] Traub, L. W., Miller, A., Rediniotis, O., "Effects of Synthetic Jet Actuation on a Ramping NACA 0015 Airfoil", *Journal of Aircraft*, Vol. 41, No. 5, 2004, pp.1153-1162.
- [3] Wang, H., Menon, S., "Fuel-Air Mixing Enhancement by Synthetic Microjets", *AIAA Journal*, Vol. 39, No. 12, 2001, pp. 2308-2319.
- [4] Pavlova, A., Amitay, M., "Electronic Cooling Using

Synthetic Jet Impingement”, *Journal of Heat Transfer*, Vol. 128, Issue 9, 2006, pp. 897-907.

[5] Greenblatt, D., Wygnanski, I., “The Control of Separation by Periodic Excitation”, *Progress in Aerospace Science*, Vol. 36, No. 7, 2000, pp. 487-545.

[6] Crook, A., Woodf, N. J., “Measurements and Visualizations of Synthetic Jets”, 39th Aerospace Sciences Meeting and Exhibit, AIAA 2001-0145, Reno, Nevada, January 2001.

[7] Feng, Li-Hao, Wang, Jin-Jun, “Particle Image Velocimetry Study of Parameter Influence for Synthetic-Jet Application”, *Flow Measurement and Instrumentation*, Vol. 34, 2013, pp. 53-67.

[8] Feng, Li-Hao, Wang, Jin-Jun, “Modification of a Circular Cylinder Wake with Synthetic jet: Vortex Shedding Modes and Mechanism”, *European Journal of Mechanics - B/ Fluids*, Vol. 43, 2014, pp. 14-32.

[9] Cannelle, F., Amitay, M., “Transitory Behavior of a Finite Span Synthetic Jet”, *Physics of Fluids*, Vol. 19, Issue 9, 094108, 2007.

[10] Amitay, M., Cannelle, F., “Evolution of Finite Span Synthetic Jets”, *Physics of Fluids*, Vol. 18, 054101, 2006.

[11] Ravi, B. R., Mittal, R., Najjar, F.M., “Study of Three-Dimensional Synthetic Jet Flowfields Using Direct Numerical Simulation, 42nd AIAA Aerospace Sciences Meeting and Exhibit, AIAA 2004-0091, Reno, NV, January 2004.

[12] Rumsey, C.L., Schaeffler, N.W., Milanovic, I.M., Zaman, K.B.M.Q., “Time-Accurate Computations of Isolated Circular Synthetic Jets in Crossflow”, *Computers & Fluids*, Vol. 36, Issue 6, 2007, pp. 1092-1105.

[13] Günther, B., Thiele, F., Petz, R., Nitsche, W., Sahner, J., Weinkauff, T., Hege, H.-C., “Control of Separation on the Flap of a Three-Element High-Lift Configuration”, 45th AIAA Aerospace Sciences Meeting and Exhibit, AIAA 2007-265, Reno, Nevada, January 2007.

[14] Petz, R., Nitsche, W., “Active Separation Control on the Flap of a Two-Dimensional Generic High-Lift Configuration”, *Journal of Aircraft*, Vol. 44, No. 3, 2007, pp. 865-874.

[15] Kim, S. H., Kim, C., “Separation Control on NACA23012 Using Synthetic Jet”, *Aerospace Science and Technology*, Vol. 13, 2009, pp. 172-182.

[16] Kim, M., Kim, S. H., Kim, W., Kim, Y., Kim, C., “Flow Control of Tilt-Rotor Airfoils Using Synthetic Jets”, *Journal of Aircraft*, Vol. 48, No. 3, 2011, pp. 1045-1057.

[17] Zhang, S., Zhong, S., “Experimental Investigation of Flow Separation Control Using an Array of Synthetic Jets”, *AIAA Journal*, Vol. 48, No. 3, 2010, pp. 611-623.

[18] Zhou, J., Zhong, S., “Numerical Simulation of the Interaction of a Circular Synthetic Jet with a Boundary Layer”, *Computers & Fluids*, Vol. 38, Issue 2, 2009, pp. 393-405.

[19] Kim, W., Kim, C., Jung, K. J., “Separation Control Characteristics of Synthetic Jets Depending on Exit Configuration”, *AIAA Journal*, Vol. 50, No. 3, 2012, pp. 559-570.

[20] Rumsey, C.L., Gatski, T.B., Sellar III, W.L., Vasta, V.N., Viken, S.A., “Summary of the 2004 CFD Validation Workshop on Synthetic Jets and Turbulent Separation Control”, 2nd AIAA Flow Control Conference, AIAA-2004-2217, Portland, Oregon, June 2004.

[21] Chorin, A. J., “A Numerical Method for Solving Incompressible Viscous Flow Problems”, *Journal of Computational Physics*, Vol. 2, Issue 1, 1967, pp. 12-26.

[22] Kim, C. S., Kim, C., Rho, O. H., “Parallel Computations of High-Lift Airfoil Flows Using Two-Equation Turbulence Models”, *AIAA Journal*, Vol. 38, No. 8, 2000, pp. 1360-1368.

[23] Yoon, S., Kwak, D., “Three-Dimensional Incompressible Navier-Stokes Solver Using Lower-Upper Symmetric Gauss Seidel Algorithm”, *AIAA Journal*, Vol. 29, No. 6, 1991, pp. 874-875.

[24] Bardina, J.E., Huang, P.G., Coakley, T.J., “Turbulence Modeling Validation, Testing and Development”, NASA TM-110446, 1997.

[25] Zheng, X., Liu, C., Liu, F., Yang, C., “Turbulent Transition Simulation Using the $k-\omega$ model”, *International Journal for Numerical Methods in Engineering*, Vol. 42, No. 5, 1998, pp. 907-926.

[26] Rumsey, C.L., “Computation of a Synthetic Jet in a Turbulent Cross Flow Boundary Layer”, NASA TM -213273, 2004.

[27] Geissler, W., “A Family of CFD Boundary Conditions to Simulate Separation Control”, *Aerospace Science and Technology*, Vol. 14, No. 7, 2010, pp. 494-504.

[28] Kral, L. D., Donovan, J. F., Cain, A.B., Cary, A.W., “Numerical Simulation of Synthetic Jet Actuators”, 4th AIAA Shear Flow Control Conference, AIAA paper 1824, Snowmass Village, USA, 1997.

[29] Duvigneau, R., Visonneau, M., “Optimization of a Synthetic Jet Actuator for Aerodynamic Stall Control”, *Computers & Fluids*, Vol. 35, Issue 6, 2006, pp. 624-638.

[30] Yang, A., “Design Analysis of a Piezoelectrically Driven Synthetic Jet Actuator”, *Smart Materials and Structures*, Vol. 18, 2009, pp. 1-12.

[31] Gallas, Q., Mathew, J., Kasyap, A., Holman, R., Nishida, T., Carroll, B., Sheplak, M., “Lumped Element Modeling of Piezoelectric-Driven Synthetic Jet Actuators”, 40th AIAA Aerospace Sciences Meeting and Exhibit, 2002-0125.

[32] Mane, P., Mossi, K., Bryant, R., “Experimental Design and Analysis for Piezoelectric Circular Actuators in Flow Control Applications”, *Smart Materials & Structures*, Vol. 17, 2009.

[33] Owen, P., Klanfer, L., “On the Laminar Boundary Layer Separation from the Leading-Edge of a Thin Aerofoil”, Aeronautical Research Council Current Papers, No. 220, 1955.

[34] Loftin, L. “Theoretical and Experimental Data for a Number of NACA 6A-Series Airfoil Sections”, Technical report of National Advisory Committee for Aeronautics, No. 903, 1947.

[35] Ziada, S., “Control of Fluid-Structure-Sound Interaction Mechanisms by Means of Synthetic Jets”, JSME International Journal, Vol. 46, No. 3, 2003, pp. 873-880.

[36] Electric Actuators for Airfoil Separation Control,” AIAA Journal, Vol. 36, No. 8, 1998, pp. 1535-1537

[37] Torenbeek, E., Wittenberg, H., “Flight Physics: Essentials of Aeronautical Disciplines and Technology with Historical Notes”, Springer, 2009, pp. 110-111.

[38] Smith, D. R., Amitay, M., Kibens, V., Parekh, D., and Glezer, A., “Modification of Lifting Body Aerodynamics Using Synthetic Jet Actuators”, AIAA Journal, 1998, pp. 98-0209.

[39] Schlichting, H., and Gersten, K., “Boundary-Layer Theory”, 8th ed., Springer-Verlag, New York, 2000, pp. 419-443.